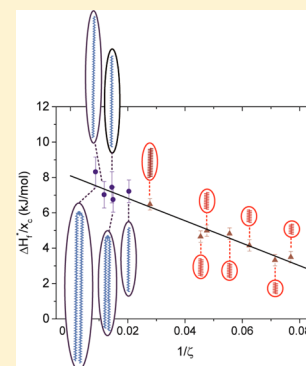


## Quantifying Crystallinity in High Molar Mass Poly(3-hexylthiophene)

Chad R. Snyder,<sup>\*,†</sup> Ryan C. Nieuwendaal,<sup>†</sup> Dean M. DeLongchamp,<sup>†</sup> Christine K. Luscombe,<sup>‡</sup> Prakash Sista,<sup>‡</sup> and Shane D. Boyd<sup>‡</sup><sup>†</sup>Materials Science and Engineering Division, National Institute of Standards and Technology, Gaithersburg, Maryland 20899, United States<sup>‡</sup>Materials Science and Engineering Department, University of Washington, Seattle, Washington 98195, United States

**ABSTRACT:** We demonstrate a method to determine absolute crystallinity in high molar mass poly(3-hexylthiophene) (P3HT), as used in commercially relevant organic photovoltaic devices, using enthalpy of fusion and melting temperature values derived from differential scanning calorimetry (DSC) and <sup>13</sup>C CPMAS NMR. By studying P3HT with molar masses ranging from 3.6 to 49 kg/mol and using recent work on oligomeric 3-hexylthiophene, we demonstrate several critical items. First, that proper extrapolation to infinite chain lengths, i.e., crystal size, yields values for the equilibrium melting temperature  $T_m^0$  of  $272 \pm 6$  °C and the enthalpy of fusion per crystalline repeat unit  $\Delta H_u$  of  $49 \pm 2$  J/g for Form I crystals of P3HT. Second, that a simple correction for crystal size using  $T_m^0$  is critical for determining an accurate degree of crystallinity from enthalpy measurements because of finite crystal size effects. Furthermore, our results demonstrate that the ordered fraction of P3HT measured from <sup>13</sup>C NMR is indistinguishable from the DSC-determined crystalline fraction, once crystal size corrections are properly implemented. The connection between crystal size and melting temperature is affirmed by successive self-nucleation and annealing (SSA) measurements, which, when performed as a function of molar mass, allowed us to identify the molar mass at which chain folding occurs in P3HT in the melt,  $\approx 11.5$  kg/mol.



## INTRODUCTION

Poly(3-hexylthiophene) (P3HT) is one of the most widely researched materials for organic thin film electronic<sup>1,2</sup> and organic photovoltaic<sup>3–6</sup> applications. It is surprising, then, that quantitative metrics for degrees of crystallinity are still lacking. Differential scanning calorimetry (DSC) has long been considered the “gold standard” for the determination of absolute crystallinity through the use of the enthalpy of fusion per mole repeat unit  $\Delta H_u$  of a perfect crystal. In recent years a number of DSC techniques, such as the one employed in this paper, have been shown to quantify endotherms for samples down to  $\approx 0.2$  mg, which is roughly the sample mass of a 2 cm  $\times$  2 cm  $\times$  100 nm polymer film. With accurate heat of fusion values as a function of molar mass, one should be able to obtain a value for  $\Delta H_u$  and, in turn, an absolute degree of crystallinity for such a film. Herein, we report a precisely determined value of  $\Delta H_u$  for P3HT and demonstrate that because of finite crystal size effects, a value for the equilibrium melting temperature  $T_m^0$ , which we also report from our measurements, is necessary for calculating crystallinity via DSC. Our measurements also allow us to show that what we previously<sup>7</sup> treated as a “noncrystalline, locally ordered” fraction of P3HT chains observed via a combination of X-ray, DSC, and <sup>13</sup>C NMR should instead be considered crystalline when properly considering the role of crystal size. The result is that crystallinities determined from DSC show good agreement with the ordered fractions from NMR.

To date, a trustworthy value of  $\Delta H_u$  for P3HT has proven difficult to obtain. The earliest reported value for  $\Delta H_u$  of 98 J/g (and for the equilibrium melting temperature  $T_m^0$  of 300 °C)

was proposed by Malik and Nandi.<sup>8</sup> However, a number of studies in recent years questioned the validity of this value, suggesting that it was far too large. Lee and Dadmun<sup>9</sup> using density and enthalpy measurements estimated a range of the enthalpy of fusion of high molar mass P3HT to be between 37 and 50 J/g, to maintain consistency with likely values for the P3HT crystal density, clearly demonstrating that the value of 98 J/g is too high. Pascui and co-workers, using solid state nuclear magnetic resonance (NMR) spectroscopy on low molar mass fractions of P3HT, proposed a value of  $\leq 37$  J/g.<sup>10</sup> A thorough study by Koch and co-workers examined the melting and crystallization of oligomers of 3-hexylthiophene (3HT)<sub>n</sub> with lengths ranging from  $n = 4$  to 36<sup>11</sup> and made estimates for the enthalpy of fusion of the two different crystal forms of P3HT of  $\approx 39$  J/g for Form I and  $\approx 70$  J/g for Form II. They also determined equilibrium melting temperatures for the Form I and Form II crystals of 571 K (298 °C) and 389 K (116 °C), respectively. Form II, in which the hexyl side chains interdigitate, has been observed only in lower molar mass samples. Finally, a recent study by Balko and co-workers<sup>12</sup> attempted to estimate the amorphous fraction in Form I crystals through X-ray diffraction and use this to compute the degree of crystallinity; however, they neglected the crystal size effect on the measured enthalpy of fusion and computed a value of 33 J/g by averaging the values for four fractions ranging from 3.2 to 24 kg/mol. For the lower molar masses, this is

Received: January 17, 2014

Revised: May 16, 2014

Published: June 3, 2014

particularly problematic since, as we will show, the enthalpy-determined degree of crystallinity is strongly affected by the crystal size and will result in values of  $\Delta H_u$  that are too low.

Both the studies of Pascui et al. and Koch et al. were performed primarily on low molar mass P3HT. There remains some question about the applicability of the extrapolations to higher molar mass. Recently, studies in our laboratory<sup>7</sup> have demonstrated that solid state NMR cannot so straightforwardly quantify the degree of crystallinity in high molar mass (Form I) P3HT when using methods previously demonstrated<sup>10</sup> on lower molar mass P3HT. Complications in side chain dynamics arise which precludes the use of side chain conformers for crystal identification. Furthermore, as we show below, the simple use of the enthalpy of fusion for crystallinity quantitation yields inaccurate results. Rather, because of observed surface enthalpy effects, crystal size must be accounted for, which can only be accomplished if the melting temperature and enthalpy of fusion of infinite chain length (crystal size) are known, which we give below. These values are determined by investigating seven P3HT fractions with relatively low dispersity ( $\bar{D} = \langle M_w \rangle / \langle M_n \rangle$ , where  $\langle M_w \rangle$  is the mass-averaged molar mass and  $\langle M_n \rangle$  is the number-averaged molar mass) with  $\langle M_n \rangle$  ranging from 3.6 to 49 kg/mol (the properties of which are given in Table 1).

**Table 1. Molecular Characteristics of P3HT Fractions**

$\langle M_n \rangle$ from NMR (kg/mol)	$\bar{D} = \langle M_w \rangle / \langle M_n \rangle$ from GPC	$\langle n \rangle$
3.6	1.30	22
5.9	1.24	35
8.2	1.15	49
11.5	1.14	69
15.9	1.18	96
23.2	1.24	140
≈49	1.90	294

## EXPERIMENTAL SECTION

**Materials.** P3HT fractions from 3.6 to 23.2 kg/mol were synthesized, purified, and characterized as described elsewhere.<sup>13</sup> Number-average molar masses  $\langle M_n \rangle$  were determined using end-group analysis via <sup>1</sup>H NMR, and size exclusion chromatography relative to polystyrene standards was used to determine the dispersity  $\bar{D}$  [Viscotek<sup>14</sup> model 305 triple detector array at 30 °C (RI, viscometer, light scattering)]; columns: Viscotek I-MBHMW-3078 (2); mobile phase: THF; flow rate: 1 mL/min; injection volume: 100  $\mu$ L]. Matrix assisted laser desorption time-of-flight (MALDI-TOF) mass spectra were recorded on a Bruker Autoflex II spectrometer using terthiophene as the sample matrix, and all P3HT fractions contained Tol/H end groups. The regioregularities of the samples were confirmed using <sup>1</sup>H NMR and were found to be ≈100%.<sup>13</sup> The ≈49 kg/mol sample was Plexcore OS2100 (Plextronics); GPC information was provided by the manufacturer, and  $\langle M_n \rangle$  was estimated via <sup>1</sup>H NMR assuming H/Br termination. The regioregularity of the commercial sample was >98%. (Table 1 summarizes the material properties.) We note that a recent study by Wong et al.<sup>15</sup> has suggested that  $\bar{D}$  determined by GPC could be an underestimate for P3HT; e.g., for the two highest molar mass samples studied this could be up to ≈35%. However, as the values of  $\bar{D}$  do not enter into any calculations, this will not be pursued further in this article. The same study also suggests that end-group analysis may begin to have problems above ≈40 kg/mol, but only the commercial sample is near this threshold and we have stated that this value is an estimate only.

**Solid State Nuclear Magnetic Resonance (NMR) Spectroscopy.** NMR experiments were performed at 2.35 T on a Tecmag Apollo spectrometer, ultrawide bore Nalorac magnet, and home-built

7.5 mm double resonance magic angle spinning probe. Each sample (≈50 mg) was slightly pressed into a 3 mm × 7 mm disk, placed into a Macor rotor, and spun at 3800 ± 100 Hz. Cross-polarization magic angle spinning (CPMAS) was performed with the following conditions: 25.19 MHz <sup>13</sup>C frequency, 100.16 MHz <sup>1</sup>H frequency, 3.2  $\mu$ s <sup>1</sup>H  $\pi/2$  pulse, 2 ms contact time, 72 kHz <sup>13</sup>C contact pulse, 68 kHz <sup>1</sup>H contact pulse, 78 kHz continuous wave (CW) decoupling, 100  $\mu$ s dwell time, 600 data points with 15 784 zero filling points, 2048–8196 scans, and 4 s recycle delay. The  $T_{1\rho}^H$  spectral editing was performed by acquiring CPMAS spectra with and without a 68 kHz 7 ms spin-lock pulse as was demonstrated previously.<sup>7</sup> The 7 ms spin-lock pulse allows the amorphous (broad, fast relaxing) component to decay, leaving a spectrum weighted in the ordered (narrow) component. The <sup>1</sup>H CW decoupling frequency was set to 3.3 ppm (relative to tetramethylsilane at 0 ppm). The CPMAS spectra are >96% quantitative. The ordered fraction estimates are obtained by taking difference spectra ( $x \times$  total measured spectrum – ordered fraction spectrum from 7 ms spin lock pulse = disordered spectrum), where  $x$  is the ordered fraction value. The estimated error ranges are obtained by iterating over range of ordered fraction estimates. A smoothness restriction, in an analogous manner that employed in regularization methods, is placed on the disordered fraction's spectrum. Thus, the error ranges are based on values at the extremes when the smoothness restriction is violated, yielding physically unreasonable difference spectra; i.e., too small a value of  $x$  would leave a positive narrow component in the difference (i.e., amorphous) spectrum, and too large a value of  $x$  would leave a negative narrow component in the difference.

**Wide-Angle X-ray Diffraction (WAXD).** WAXD measurements on the same disks prepared for the NMR measurements were performed on a Rigaku Smartlab at 40 kW and 40 mA with a Cu K $\alpha$  radiation (wavelength  $\lambda = 0.154$  nm) using a D/tex Ultra semiconductor high-speed detector with 0.01° steps at 3 s for each step. A Bragg–Brentano geometry was used with a sample to detector distance of 175.5 mm; a 0.3 mm detector slit was used, resulting in an ≈0.05° full width at half-maximum Gaussian instrument profile function. As this was considerably less than the widths of the peaks it was neglected in the study.

**Differential Scanning Calorimetry (DSC).** DSC was performed on a PerkinElmer DSC8500 equipped with a helium purge and a CLN2 liquid nitrogen chiller. Measurements were performed in HyperDSC mode<sup>16,17</sup> on multiple samples with masses ranging from 0.2 to 0.8 mg enclosed in aluminum foil packets with masses of ≈1.9 mg. Unless otherwise specified, heating was performed at 100 °C/min; temperature calibration was achieved using indium and lead standards of similar masses in foil packets. The high heating rates were used to (1) enable reduced total sample usage and (2) reduce the possibility of melting/recrystallization. Measurements on the as-synthesized 15.9 kg/mol sample at both 10 and 100 °C/min yielded identical values for the enthalpy and melting temperatures within the experimental uncertainty. Successive self-nucleation and annealing (SSA) measurements were performed with heating and cooling rates of 10 °C/min with 5 min holds at the annealing temperatures and 1 min holds at 20 °C; only the final heating scan was performed at 100 °C/min. SSA at high heating rates has been demonstrated by Pijpers and Mathot.<sup>18</sup>

## RESULTS AND DISCUSSION

The enthalpy of fusion as a function of polymer crystal thickness in the chain axis direction ( $\zeta$ ) can be written approximately as<sup>19</sup>

$$\frac{\Delta H_f^*}{x_c} \cong \Delta H_u + \frac{\Delta H_e}{\zeta} \quad (1)$$

where  $\Delta H_f^*$  is the measured enthalpy of fusion per mole of repeat unit,  $x_c$  is the crystalline mass fraction, and  $\Delta H_e$  is the enthalpic penalty due to chain ends (or enthalpic contribution to the interfacial free energy); extrapolation to infinite molar mass (crystal thickness) therefore yields the crystal repeat unit

enthalpy of fusion in the absence of the chain ends (or crystal/amorphous interfacial region). The equation, developed by Broadhurst,<sup>20</sup> that Koch and co-workers used for their analysis of the oligomer series for the observed melting temperature  $T_m$  as a function of chain length  $n$  is<sup>20</sup>

$$T_m = T_m^0 \frac{n + a}{n + b} \quad (2)$$

where  $a$  and  $b$  are constants, with  $a$  approximately equal to

$$a \cong \frac{\Delta H_e}{\Delta H_u} \quad (3)$$

(Note that the term  $\Delta H_e/\zeta$  in eq 1 was written as  $2\Delta H_e/\zeta$  in the original reference; however, we cast it in the current form for consistency with Broadhurst's derived relationship.)

Before analyzing our data using these equations, we considered two important points that were raised by Koch and co-workers.<sup>11</sup> First, we had to identify whether our samples consisted of Form I or II crystals or a combination of the two. Second, we needed to address the issue of dispersity  $\mathcal{D}$  and its impact on the thermal properties. In nearly all cases, and unless otherwise indicated, the measurements were performed on the as-synthesized and purified fractions because it is our experience that these tend to have the highest degree of crystallinity. Figure 1 is a plot of the wide-angle X-ray

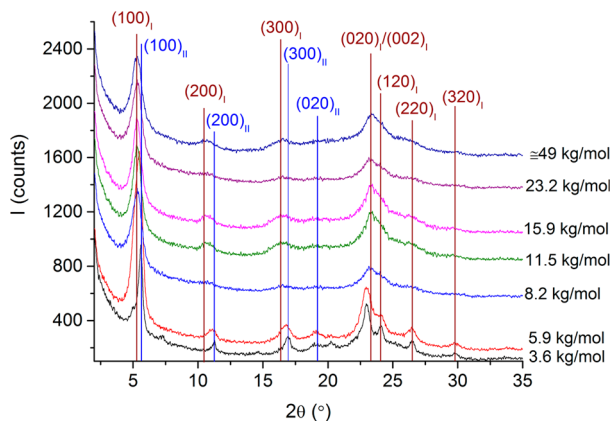


**Figure 1.** Typical WAXD patterns taken from samples of the as-synthesized powder lightly pressed into cylinders. The curves have been offset vertically for clarity. The peaks were indexed based on the literature for Form I<sup>21–23</sup> and Form II.<sup>11,21,24,25</sup>

diffraction (WAXD) data for each of our synthesized fractions, with several of the expected peak positions for each of the crystal forms labeled on the plot. It is clear that for the fractions 3.6 and 5.9 kg/mol we have both Form I and II crystals as shown by the shifts in the  $(h00)$  peaks, and for 8.2–49 kg/mol it is primarily Form I.

To examine the impact and extent of chain fractionation, we used successive self-nucleation and annealing (SSA).<sup>26</sup> SSA is a thermal processing and analysis technique that bins chains into specific crystal size populations corresponding to discrete crystallizable sequence lengths that can then be quantified by discrete melting peak temperatures and enthalpies. The melting peak temperature for each discrete endotherm in an SSA analysis provides the crystallizable sequence length, which when combined with the enthalpy of the peak can be used to correlate the crystal size with the mass fraction of each discrete grouping of crystal sizes. In the case of regiodeficient P3HT,

crystallizable segments correspond to chain lengths between defects since the regiodeficient appear to be excluded from the crystal.<sup>27,28</sup> In the case of 100% regioregular P3HT only chain ends are excluded. The SSA process works by first destroying existing homogeneous nuclei by heating to a temperature in excess of the melting temperature ( $T_m'$ ), followed by cooling at a constant rate to some lower reference temperature ( $20\text{ }^\circ\text{C}$  in our case). Then the sample is heated, at the same constant rate at which the sample was cooled, to a self-seeding temperature ( $T_s$ ) and annealed for 5 min, which results in partial melting and potential annealing of unmelted crystals as well as isothermal crystallization. Subsequent replicates of cooling to the reference temperature followed by heating to decreasing annealing temperatures results in formation of discrete populations of fixed crystallizable sequence lengths that are thermodynamically stable between the annealing temperatures; in our case this corresponds to a  $5\text{ }^\circ\text{C}$  separation in annealing temperatures. Upon completion of the final annealing step, the sample is cooled to a sufficiently low temperature to capture the entire melting process and the sample is heated for the last time, and the resulting final DSC trace provides a “report” of the fractions produced. Note that sharp fractions (peaks) will only be produced in the case of extended chain crystals of oligomers or in copolymers where there are sequences of noncrystallizable monomers. When chain folded crystals can form, the distribution of crystal thicknesses produced will be continuous rather than discrete. Figure 2 summarizes the SSA procedure used in this paper.

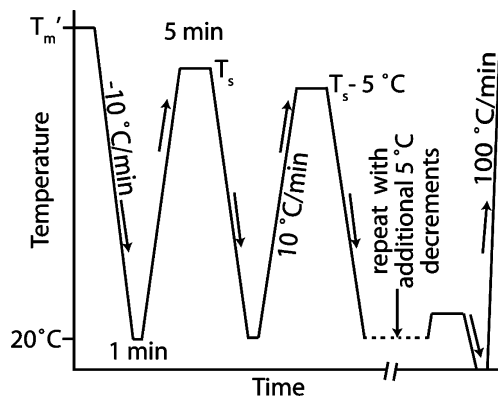


**Figure 2.** Self-nucleation and annealing process used to characterize the P3HT fractions.  $T_m'$  was typically chosen to be on the order of  $25\text{ }^\circ\text{C}$  above the melting temperature of the fractions, and the sample was held in the melt for 3 min initially. Note that all heating and cooling rates were  $10\text{ }^\circ\text{C}/\text{min}$ , except for the final heating trace that was performed at  $100\text{ }^\circ\text{C}/\text{min}$ .

The results of the fractionation studies, shown in Figure 3, indicate that for the samples of 11.5 kg/mol and lower significant fractionation occurred. For the samples of 15.9 kg/mol and higher, no appreciable fractionation was present; i.e., sharp discrete peaks with  $\approx 5\text{ }^\circ\text{C}$  spacing are not formed. This indicates that, for the three highest molar mass samples, chain folding occurs under appropriate conditions. (It should be mentioned also that a DSC scan (not shown) obtained on a sample of the 11.5 kg/mol after fast cooling is strongly suggestive of a transition from once folded to extended chain as was seen by Ungar and co-workers<sup>29</sup> for  $n\text{-C}_{294}\text{H}_{590}$ .) This is consistent with the results of Koch and co-workers,<sup>30</sup> who established that the onset of chain folding was occurring

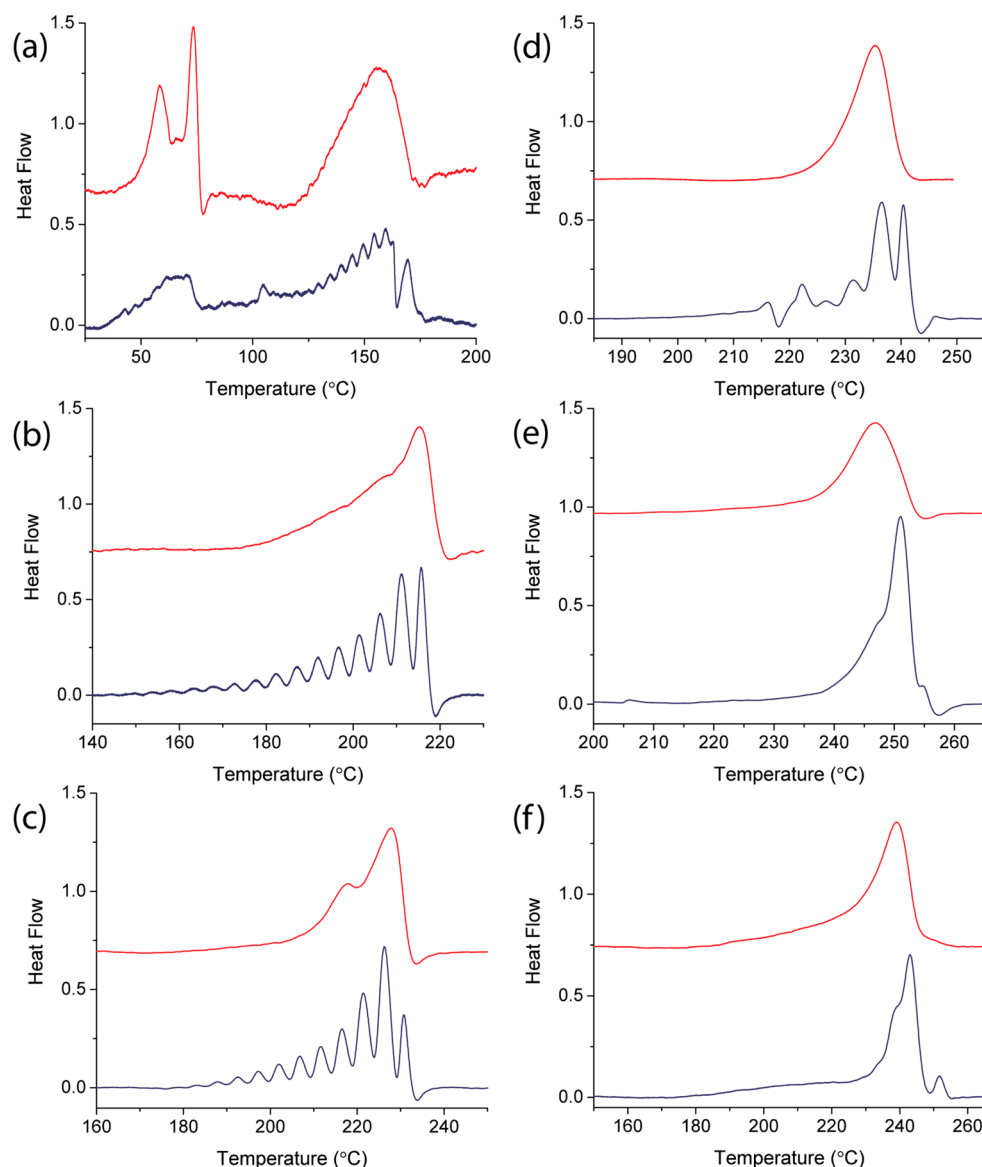


**Figure 3.** Typical first pass DSC traces (upper curves) and self-nucleation and annealing (SSA) DSC traces (lower curves) for the synthesized fractions (a) 3.6, (b) 5.9, (c) 8.2, (d) 11.5, (e) 15.9, and (f) 23.2 kg/mol. Endotherm direction is up. Traces have been passed through a Savitsky–Golay filter for smoothing, and baseline curvature effects have been subtracted for clarity.

between 8 and 25 kg/mol (polystyrene equivalent molar mass), Brinkman and Rannou,<sup>31</sup> who placed it between  $\langle M_w \rangle = 7.3$  and 18.8 kg/mol (polystyrene equivalent molar mass), and the work of Liu and co-workers,<sup>32</sup> who placed it between  $\langle M_n \rangle = 10.2$  and 15.6 kg/mol (polystyrene equivalent molar mass). However, due to our use of SSA and closer fraction spacing, we have tightened this range considerably down to an approximate value of  $\approx 11.5$  kg/mol. We note that Balco and co-workers<sup>12</sup> recently estimated the transition between  $\langle M_n \rangle = 12.4$  and 17.5 kg/mol (MALDI determined molar mass) using changes in the long period from small-angle X-ray scattering because the 12.4 kg/mol sample still demonstrated a long period attributable to an extended chain conformation; however, as shown by Ungar and co-workers at the critical molar mass for onset of chain folding both chain folded and extended chain crystals can form under appropriate circumstance as indicated by the exotherms in the SSA analysis of our 11.5 kg/mol fraction. (We feel it important to clarify our view of chain folding in P3HT to address what may be a misconception related to the folding

process. Unlike in polyethylene where the fraction of *tight* chain folds, i.e., not “hairpin” folds but the fraction of folds which include adjacent folds, near-adjacent folds, and next-nearest-adjacent folds, is considered to be  $>2/3$ , it can be estimated via the Gambler’s Ruin approach (see Appendix II) that for melt processed P3HT this number is expected to be quite smaller, i.e., on the order of  $<20\%$ .)

The five highest molar mass samples ( $\langle M_n \rangle \geq 8.2$  kg/mol) were used for enthalpy characterization since WAXD showed primarily Form I. However, as shown in Figure 3, the SSA analysis showed that the largest endotherms for the samples that did not undergo chain folding (Figure 3a–d) were nearly coincident with the endotherm peak measured by a first-heat DSC measurement on the as-synthesized samples and thus could be used for the melting point analysis ( $\langle M_n \rangle \leq 11.5$  kg/mol).

In Figure 4, we plot the melting points of oligomeric 3HT from Koch and co-workers as well as the melting points of our four lower molar mass P3HT fractions 3.6–11.5 kg/mol, which

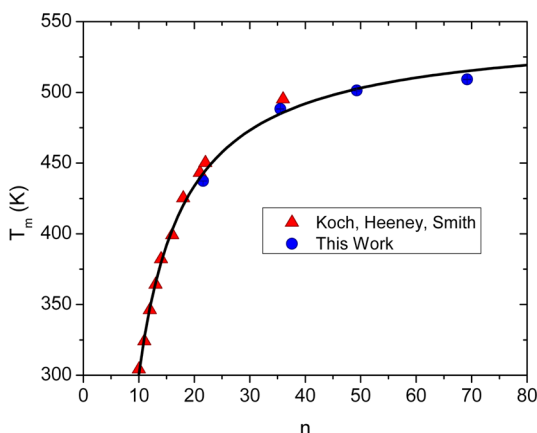


**Figure 4.** Melting temperature ( $T_m$ ) as a function of number of repeat units. The data from Koch, Heeney, and Smith are taken from ref 11. Error bars corresponding to one standard deviation in the experimental data on our data are smaller than the symbol size. The curve is a nonlinear least-squares fit to eq 2 using  $1/\text{standard deviation}$  as a weighting factor. For the data of Koch and co-workers we assumed an uncertainty of  $\pm 0.25$  °C.

do not undergo chain folding. It is clear that our data overlap well with their data at shorter chain lengths. Our fit using eq 2 to the data results in  $T_m^0 = 545 \pm 6$  K (272 °C),  $a = -5.4 \pm 0.5$ , and  $b = -1.6 \pm 0.4$ , with the error estimates being the best estimate of one standard deviation derived from the covariance matrix of the fit. The equilibrium melting temperature determined from our fit is 26 °C less than the value provided by Koch and co-workers, which illustrates that higher molar mass samples are needed to fully capture the curvature in the data.

To determine the estimates of the (locally) ordered fraction as a function of chain length, we acquired  $^{13}\text{C}$  cross-polarization magic angle spinning (CPMAS) NMR spectra of our sample set. The ordered and disordered mass fractions were deconvolved based on  $T_{1\rho}^H$  differences and aromatic resonance chemical shift contrast.<sup>7</sup> (Figures 5a–g are plots of the spectra for the molar masses studied, and Figures 5h–j show an example of the deconvolution into ordered and disordered components.) Since no appreciable spectral separation was observed between the ordered and disordered P3HT methyl resonances, previously published methods<sup>10</sup> for crystallinity determination could not be applied. This lack of spectral contrast in Form I P3HT is suggestive of similar time-averaged ( $\approx 3$  ms) populations of side-chain conformers (anti vs gauche methylenes) existing in the crystalline and noncrystalline phases, unlike Form II P3HT.

We showed previously, based on comparisons to XRD and DSC measurements, that in some cases noncrystalline chains can be locally ordered, but no crystalline polymer would be excluded from the NMR-determined “ordered fraction”.<sup>7</sup> While we discuss further details of this assertion below, for the following analysis the ordered fraction characterized by NMR is utilized for an upper bound on the degree of crystallinity. Table 2 summarizes the measured ordered fractions and enthalpies.

In Figure 6, we have plotted enthalpy as a function of inverse crystal size for both our data (blue circles) as well as the oligomeric data from Koch and co-workers (red triangles). The enthalpy has been normalized by crystalline mass fraction ( $x_c$ ) for both sets of data, but for monodisperse oligomeric systems such as those studied by Koch et al.,  $x_c = 1$  is assumed. In

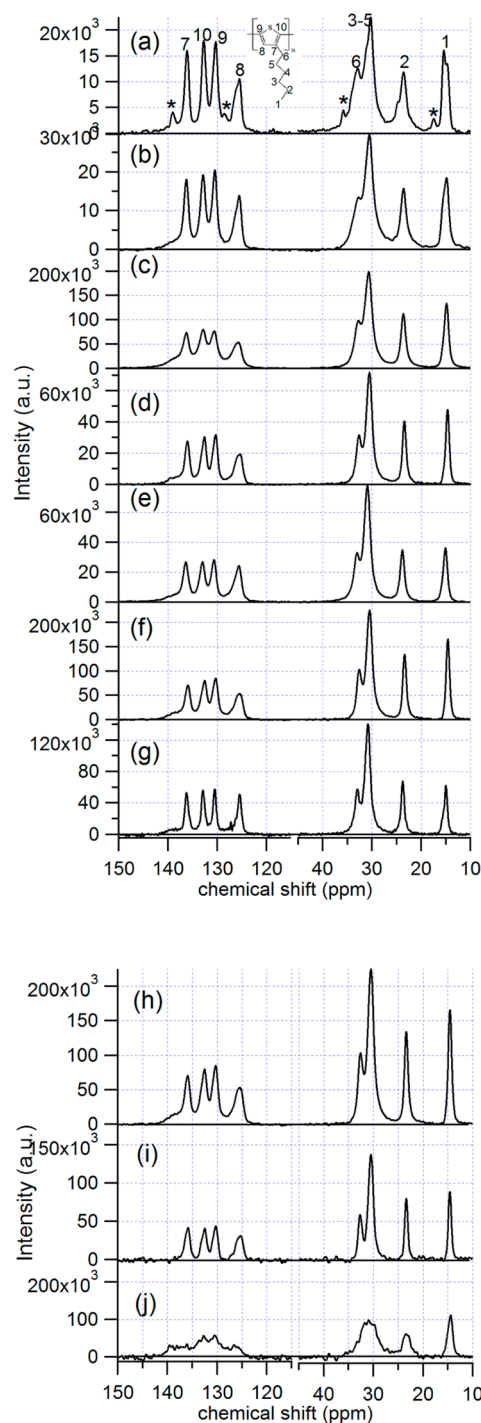


**Figure 5.** (a–g)  $^{13}\text{C}$  CPMAS NMR spectra of P3HT with varied molar mass (kg/mol): (a) 3.6, (b) 5.9, (c) 8.2, (d) 11.5, (e) 15.9, (f) 23.2, and (g)  $\approx 49$ . (h–j)  $^{13}\text{C}$  CPMAS spectra of 23.2 kg/mol P3HT (h) and its ordered (i) and disordered (j) fractions. The asterisks given in (a) are tolyl end-group resonances.

higher molar mass P3HT, a crystallinity value cannot be assumed, but a lower bound can be placed based on  $\Delta H_f^*/x_c$  from our NMR measurements. Since no crystallinity correction need be made for the Koch data, fits were performed to eq 1. In fitting to the data, we chose to exclude the oligomers with  $n < 13$ , since as Koch and co-workers point out “oligomers of  $n \geq 13$  could not be prepared in Form II from the melt by thermal treatment and annealing”, suggesting those oligomers will

**Table 2.** Measured Enthalpies of Fusion ( $\Delta H_f^*$ ) and Their Associated Total Ordered Fraction and Line Width Data from CPMAS Measurements

$\langle M_n \rangle$ from NMR (kg/mol)	$\zeta^c$	$\Delta H_f^*$ (J/g)	$x_c$ DSC <sup>d</sup> corrected for finite crystal size	NMR ordered fraction	C7 chemical shift (ppm)	line width (ppm)
3.6	22	n/a <sup>b</sup>	n/a <sup>b</sup>	0.67	136.1	1.11
5.9	35	n/a <sup>b</sup>	n/a <sup>b</sup>	0.65	136.2	1.14
8.2	49	28.2 ± 1.8	0.62 ± 0.06	0.65	136.1	1.63
11.5	69	28.2 ± 2.8	0.67 ± 0.08	0.63	136.0	1.06
15.9	85	28.3 ± 2.5	0.59 ± 0.10	0.67	136.3	1.35
23.2	67	21.1 ± 1.5	0.46 ± 0.09	0.52	135.9	1.24
23.2 (annealed) <sup>a</sup>	n/a	n/a	0.62 ± 0.11	0.60		1.14
≈49	114	28 ± 2	0.61 ± 0.12	0.56	136.2	0.82

<sup>a</sup>The sample labeled 23.2 kg/mol (annealed) was annealed at 200 °C for 6 h. The annealing produced a bimodal distribution in the DSC trace, so neither a crystal thickness nor a  $\Delta H_f^*$  value is provided. <sup>b</sup>The enthalpies for the two lowest molar mass fractions are not provided as they were not used in the enthalpy analysis due to the presence of Form II crystals. <sup>c</sup>Crystal thickness  $\zeta$  (in units of repeat units) was computed from  $\langle M_n \rangle$  for the fractions 3.6–11.5 kg/mol and was estimated from the observed melting temperatures and the Broadhurst equation (eq 2) for fractions 15.9–49 kg/mol due to the onset of chain folding. <sup>d</sup>DSC mass fraction crystallinity was computed as described in the main text using the  $T_m^0/T_m$  correction to the DSC heat flow prior to integration and the value for  $\Delta H_u$  obtained from the oligomer only data with  $n \geq 13$ . Note: these values are *not* based on the enthalpy  $\Delta H_f^*$  provided in the table.

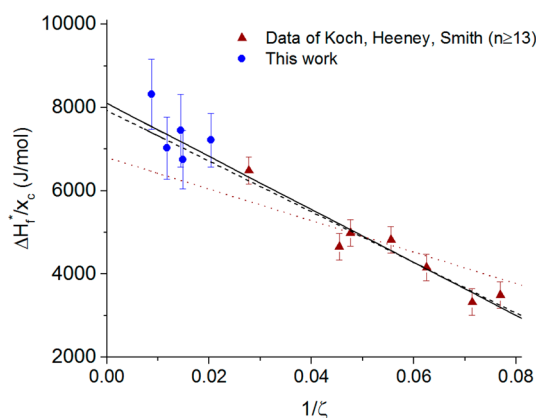


**Figure 6.** Enthalpy of fusion (measured enthalpy  $\Delta H_f^*$  divided by the mass fraction of crystallinity  $x_c$ ) as a function of inverse crystal size (in units of repeat units).  $x_c = 1$  for the oligomer data of Koch et al.<sup>11</sup> The crystal size for the data of Koch et al. was the oligomer length, and for our data the crystal size is the number-averaged chain length for fractions  $\leq 11.5$  kg/mol, and for fractions  $\geq 15.9$  kg/mol it is computed based on the observed melting temperature and eq 2 (see Table 2). The error bars on our data correspond to the best estimate of one standard deviation in the experimental uncertainty. The error bars on the Koch et al. data are based on the standard error to a linear fit of their data only. The red dotted line is a fit to the entire data set of Koch et al. (including  $n < 13$ ), the dashed line is a fit only to the data of Koch et al. for  $n \geq 13$ , and the solid line fit is the result of a weighted linear least-squares analysis to our data plus the data of Koch et al. for  $n \geq 13$ .

clearly not have any Form II “contamination”, and since the  $n < 13$  fractions showed nearly chain length independent values for the enthalpy. As shown in that previous work, and as we have found here, the low molar mass P3HT fractions are often mixed in Form I and Form II crystals, which make these data likely unreliable.

The  $\Delta H_u$  and  $\Delta H_e$  values that result from a fit to the oligomer data alone (with  $n \geq 13$ ) are  $7.9 \pm 0.5$  kJ/mol and  $-61 \pm 8$  kJ/mol, respectively (dashed line in Figure 6). For the combined data set of the oligomer data plus our data the  $\Delta H_u$  and  $\Delta H_e$  values that result from the weighted least-squares fit (solid line in Figure 6) are  $8.1 \pm 0.3$  kJ/mol and  $-64 \pm 5$  kJ/mol, respectively, which are indistinguishable from the values from the oligomer data set that have larger uncertainties. Both

of these fits are quite different from the fit to the oligomer data including the  $n < 13$  (red dotted line in Figure 6). Until this point we have treated the ordered fraction from NMR as the crystalline fraction. If it is treated as an upper bound on crystallinity, then one would obtain our data (blue circles in Figure 6) or values even higher since the blue circles could be thought of as a lower bound on  $\Delta H_f^*/x_c$ . The good agreement between the fits with (solid line) and without (dashed line) our data supports our decision in this case to use the ordered fraction of NMR as the crystalline fraction. The apparent discrepancy with the conclusions of our earlier NMR analyses will be shown later to have been an effect of crystal size. This revised value for  $\Delta H_u = 49 \pm 2$  J/g is significantly higher than that of 37 J/g of Pascui et al., 39 J/g reported by Koch and co-workers, and 33 J/g reported by Balko and co-workers. We have shown that the lower value of Koch and co-workers was due to the three lowest molar mass fractions ( $n < 13$ ), which had displayed effectively constant enthalpies that were independent of chain length and which when those values were excluded the extrapolation of their data alone yielded  $\Delta H_u = 48 \pm 3$  J/g, which is statistically indistinguishable from our new value. The data of Pascui et al. would not be expected to agree with our values as their materials were composed of Form II crystals and they did not perform a crystal size correction. Finally, the crystallinities determined by Balko and co-workers were greater than any of our observed crystallinities. One possible origin for this discrepancy was identified by Manderkern,<sup>39</sup> who demonstrated that X-ray and density values for crystallinity include the crystal–amorphous interfacial region whereas DSC and Raman values include only the crystalline core. In the systems studied by Mandelkern the interfacial region could account for 5–20% of the total sample, which if a region of similar magnitude existed in P3HT it would shift all of the crystallinities of Balko and co-workers down into the range that we obtained. Additionally, the crystal size correction would need to be applied to their enthalpy data after correction of the X-ray crystallinity for the interfacial region as the lowest molar mass sample studied by Balko and co-workers was 3.2 kg/mol, which corresponds to  $\langle n \rangle = 19$ . For a similar oligomer sample measured by Koch and co-workers,  $n = 18$ , the enthalpy for this fraction was 29 J/g, which is  $\approx 60\%$  of their revised extrapolated  $\Delta H_u$  value of 48 J/g.

The agreement of our data (with no assumed crystallinity, only a locally ordered fraction from NMR) with the dashed line fit of the data of the oligomer only data of Koch and co-workers questions how correlated the NMR-determined ordered fraction are to the absolute crystallinity measurement. With DSC-determined values of  $\Delta H_f^*$  and our values for  $\Delta H_u$  and  $T_m^0$ , one can readily calculate crystallinity, corrected for crystal size, using a previously determined analytical form from Crist.<sup>33</sup>

$$x_c \cong \frac{\Delta H_f^* T_m^0}{\Delta H_u T_m} \quad (4)$$

(Appendix I has a brief derivation showing the origin of this relationship. To properly employ this equation, the heat flow from the DSC signal should be multiplied by  $T_m^0/T_m$  prior to integration.) We have plotted in Figure 7 the crystallinity

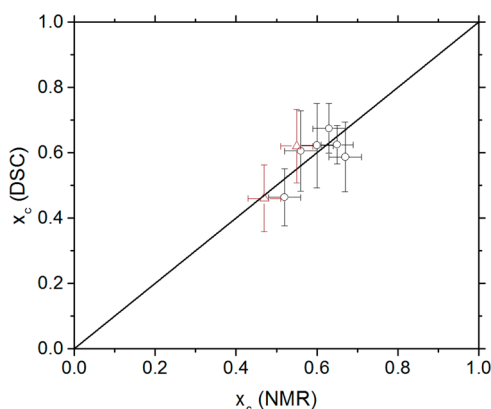


**Figure 7.** Mass fraction crystallinity estimated from  $^{13}\text{C}$  CPMAS NMR vs that estimated from DSC. *y*-axis error bars correspond to the best estimate of one standard deviation in the experimental uncertainty, and *x*-axis error bars correspond to the most likely range of ordered fraction values obtained by iterating over range estimates and implementing a smoothness restriction on the disordered P3HT fraction  $^{13}\text{C}$  CPMAS NMR line shape. Black circles correspond to fractions studied in this paper, and the red triangles correspond to the “fast cast” and “slow dried” samples from our previous work.<sup>7</sup>

calculated from DSC using eq 4 and the value of  $\Delta H_u$  obtained from the fit only to the oligomer data as a function of the ordered fraction calculated from NMR. The data overlap the solid line that corresponds to one-to-one agreement, indicating a strong correlation in the DSC-determined crystallinity and the NMR-determined “locally ordered fraction”. This suggests that the ordered fractions of chains as measured from the relative intensities of the narrow aromatic resonances in the  $^{13}\text{C}$  NMR are in fact crystalline. Furthermore, we have included the highly disordered “fast cast” and more ordered “slow dried” high molar mass P3HT samples from our previous study<sup>7</sup> on this plot (red triangles), and the agreement is quite good.

This finding causes us to reconsider our previous assertion that local order could be observed in noncrystalline regions in P3HT from  $^{13}\text{C}$  NMR. To frame this discussion, we crudely consider the enthalpic contributions to melting as originating from either intramolecular (chain conformation, ring coplanarity) or intermolecular ( $\pi$ -stacking, side-chain mixing) effects. In crystals, intramolecular order is a strict prerequisite for intermolecular order. The converse is not necessarily true, although intermolecular ordering may certainly stabilize or promote simultaneous intramolecular ordering. In our previous NMR work, we identified “locally-ordered, but noncrystalline”

chains that had a local packing environment similar to that within the crystal. It is more consistent to instead assign these chains to small, defective crystals that exhibit large degrees of disorder in the (100) and (020) crystal directions and small dimensionalities in the (001) direction so as to result in decreased  $T_m$ , with appropriately reduced values of  $\Delta H_f^*$ . Thus, they are not entirely lacking in intermolecular order; i.e., they are not “noncrystalline”. It is likely that packing defects broaden the  $^{13}\text{C}$  NMR line shape, and significantly reduce the XRD (*h*00) and (0*k*0) reflections, but do not result in decreased absolute crystallinity values as determined from DSC and NMR. Since the XRD intensity can be reduced without a corresponding change to crystallinity by DSC, we can conclude that intramolecular order is a significant contributor to the melting enthalpy. NMR is thus an excellent probe of aspects of order that contribute strongly to the melting enthalpy in P3HT. Because of the fact that we studied nearly 100% regioregular P3HT, the effects of regiodefects on the degree of crystallinity and melting temperature can be properly accounted for as we described elsewhere.<sup>27</sup>

## CONCLUSIONS

By combining melting temperature and enthalpy data from oligomers of 3-hexylthiophene with those obtained on fractions of  $\approx 100\%$  regioregular P3HT, we have established a method for determining crystallinity in P3HT. We provide relationships for melting temperature and enthalpies as a function of molar mass extending from oligomers with chain lengths of only 13 repeat units up to the high molar masses of technologically relevant P3HT. The agreement between DSC-determined absolute crystallinity and the NMR-determined ordered fraction indicates that either DSC or  $^{13}\text{C}$  NMR can be utilized for determining absolute crystallinity. Using self-nucleation and annealing, we have demonstrated that (1) melting temperature versus chain length relationships can be used to obtain information on crystallizable sequence length distributions in P3HT and (2) the molar mass at which chain folding begins to occur in P3HT is  $\approx 11.5$  kg/mol.

## APPENDIX I. DERIVATION OF CRYSTAL SIZE CORRECTION RELATIONSHIP

It was shown by Crist<sup>33</sup> through the Gibbs–Thomson equation that  $T_m^0/T_m$  could be used to correct for crystal size. This can also be shown via the Broadhurst equation. If we rewrite eq 1 as

$$\frac{\Delta H_f^*}{x_c \Delta H_u} = 1 + \frac{\Delta H_e}{\Delta H_u \zeta} = 1 + \frac{a}{\zeta} \quad (5)$$

and rewrite eq 2 as

$$\begin{aligned} \frac{T_m}{T_m^0} &= \frac{1 + a/\zeta}{1 + b/\zeta} = \left(1 + \frac{a}{\zeta}\right) \left[1 - \left(\frac{b}{\zeta}\right) + \left(\frac{b}{\zeta}\right)^2 - \dots\right] \\ &\cong 1 + \frac{a}{\zeta} \end{aligned} \quad (6)$$

and if we equate the two equations we determine

$$\frac{\Delta H_f^*}{x_c \Delta H_u} \cong \frac{T_m}{T_m^0} \quad (7)$$

and therefore

$$x_c \cong \frac{\Delta H_f^* T_m^0}{\Delta H_u T_m} \quad (8)$$

So  $T_m^0/T_m$  should be used to scale the measured enthalpy curve to approximately account for crystal size effects.

## ■ APPENDIX II. GAMBLER'S RUIN EVALUATION OF CHAIN FOLDING AND TIE CHAINS IN P3HT

Before performing the computation, it is important to point out that these computations assume an infinite chain length and are therefore not directly applicable to the fractions studied; however, the assumption of infinite chain length simplifies the computations markedly and thus reduces the total number of input parameters. The Gambler's Ruin problem is a well-studied problem in mathematical statistics<sup>34</sup> based on a random walk, where in this specific application<sup>35</sup> a tie chain corresponds to a random walk from one crystal that reaches a separate crystal at a distance  $M$  away and a fold corresponds to a random walk that returns to the same crystal. To compute the probability of tight folds, we first employ the Gambler's Ruin result<sup>35</sup> to compute a cluster size  $(1 + f)$  of chain stems formed by adjacent, near-adjacent, and next-nearest-adjacent re-entry folds as

$$1 + f = \frac{\rho_c}{\rho_a} \left( \frac{M}{1 - \alpha} + 1 \right) \left( \frac{1}{M + 1} \right) - 1 \quad (9)$$

where  $\rho_c$  is the crystal density,  $\rho_a$  is the amorphous density,  $M$  is the amorphous layer thickness ( $l_a$ ) in units of the persistence length ( $l_p$ ),  $M = l_a/l_p$ , and  $\alpha$  is a transition probability that for an isotropic amorphous region is equal to  $2/3$ . The stiffness of chains in the Gambler's Ruin approach has been accounted for by putting  $M$  in units of  $l_p$ , since at this scale, the chains can be approximated as a freely jointed chain.<sup>36</sup> The probability of a tight fold ( $P_{tf}$ ), which again includes adjacent, near-adjacent, and next-nearest-adjacent re-entry, is then given by

$$P_{tf} = 1 - \frac{1}{1 + f} \quad (10)$$

Using  $\rho_c = 1.13 \text{ g/cm}^3$ ,  $\rho_a = 1.09 \text{ g/cm}^3$ ,<sup>9</sup> and  $l_p = 2.9 \text{ nm}$ <sup>37</sup> and estimating  $l_a \approx 4 \text{ nm}$  (based on SAXS measurements of long period and ellipsometric estimates of ordered fraction)<sup>38</sup> results in  $P_{tf} \approx 0.19$ , which is considerably lower than the high probability (0.67) of tight folding in polyethylene. It should be realized that for crystals formed in dilute or semidilute solutions  $M$  could be considerably higher as the crystals are separated by a far larger distance, and hence the expected degree of tight folding could be higher, in fact on the order of polyethylene. Because of its suspected relevance to the electrical transport properties of P3HT, we also compute the theoretical probability of a tie chain (or bridge) via

$$P_{\text{bridge}} = \frac{1}{M + 1} \quad (11)$$

Using the above assumptions,  $P_{\text{bridge}} = 0.42$ . This value for  $P_{\text{bridge}}$  is considerably higher than the estimate for polyethylene, which due to polyethylene's larger value of  $M$  is on the order of 0.1, and is expected to be good for P3HT's charge transport between discrete crystals.

## ■ AUTHOR INFORMATION

### Corresponding Author

\*E-mail: chad.snyder@nist.gov (C.R.S.).

## Notes

The authors declare no competing financial interest.

## ■ ACKNOWLEDGMENTS

The authors thank L. Richter, R. J. Kline, B. Collins, H. Ro, and C. Soles for valuable discussions. This work was supported by the NSF CAREER Award (DMR 0747489).

## ■ REFERENCES

- (1) Klauk, H. *Chem. Soc. Rev.* **2010**, *39*, 2643–2666.
- (2) Reese, C.; Roberts, M.; Ling, M.; Bao, Z. *Mater. Today* **2004**, *7*, 20–27.
- (3) Thompson, B. C.; Fréchet, J. M. J. *Angew. Chem., Int. Ed.* **2008**, *47*, 58–77.
- (4) Cheng, Y.-J.; Yang, S.-H.; Hsu, C.-S. *Chem. Rev.* **2009**, *109*, 5868–5923.
- (5) Nelson, J. *Mater. Today* **2011**, *14*, 462–470.
- (6) Ruderer, M. A.; Muller-Buschbaum, P. *Soft Matter* **2011**, *7*, 5482–5493.
- (7) Nieuwendaal, R. C.; Snyder, C. R.; DeLongchamp, D. M. *ACS Macro Lett.* **2014**, *3*, 130–135.
- (8) Malik, S.; Nandi, A. K. *J. Polym. Sci., Part B: Polym. Phys.* **2002**, *40*, 2073–2085.
- (9) Lee, C. S.; Dadmun, M. D. *Polymer* **2014**, *55*, 4–7.
- (10) Pascui, O. F.; Lohwasser, R.; Sommer, M.; Thelakkat, M.; Thurn-Albrecht, T.; Saalwächter, K. *Macromolecules* **2010**, *43*, 9401–9410.
- (11) Koch, F. P. V.; Heeney, M.; Smith, P. J. *Am. Chem. Soc.* **2013**, *135*, 13699–13709.
- (12) Balko, J.; Lohwasser, R. H.; Sommer, M.; Thelakkat, M.; Thurn-Albrecht, T. *Macromolecules* **2013**, *46*, 9642–9651.
- (13) Bronstein, H. A.; Luscombe, C. K. *J. Am. Chem. Soc.* **2009**, *131*, 12894–12895.
- (14) Certain commercial equipment, instruments, or materials are identified in this paper in order to specify the experimental procedure adequately. Such identification is not intended to imply recommendation or endorsement by the National Institute of Standards and Technology, nor is it intended to imply that the materials or equipment identified are necessarily the best available for the purpose.
- (15) Wong, M.; Hollinger, J.; Kozycz, L. M.; McCormick, T. M.; Lu, Y.; Burns, D. C.; Seferos, D. S. *ACS Macro Lett.* **2012**, *1*, 1266–1269.
- (16) Mathot, V. B. F.; Goderis, B.; Scherrenberg, R. L.; van der Vegte, E. W. *Macromolecules* **2002**, *35*, 3601–3613.
- (17) Vanden Poel, G.; Mathot, V. B. F. *Thermochim. Acta* **2006**, *446*, 41–54.
- (18) Pijpers, M. F. J.; Mathot, V. B. F. *J. Therm. Anal. Calorim.* **2008**, *93*, 319–327.
- (19) Mandelkern, L.; Allou, A. L.; Gopalan, M. R. *J. Phys. Chem.* **1968**, *72*, 309–318.
- (20) Broadhurst, M. G. *J. Chem. Phys.* **1962**, *36*, 2578–2582.
- (21) Wu, Z.; Petzold, A.; Henze, T.; Thurn-Albrecht, T.; Lohwasser, R. H.; Sommer, M.; Thelakkat, M. *Macromolecules* **2010**, *43*, 4646–4653.
- (22) Colle, R.; Grosso, G.; Ronzani, A.; Zicovich-Wilson, C. M. *Phys. Status Solidi B* **2011**, *248*, 1360–1368.
- (23) Dudenko, D.; Kiersnowski, A.; Shu, J.; Pisula, W.; Sebastiani, D.; Spiess, H. W.; Hansen, M. R. *Angew. Chem., Int. Ed.* **2012**, *51*, 11068–11072.
- (24) Kayunkid, N.; Uttiya, S.; Brinkmann, M. *Macromolecules* **2010**, *43*, 4961–4967.
- (25) Rahimi, K.; Botiz, I.; Stingelin, N.; Kayunkid, N.; Sommer, M.; Koch, F. P. V.; Nguyen, H.; Coulembier, O.; Dubois, P.; Brinkmann, M.; Reiter, G. *Angew. Chem., Int. Ed.* **2012**, *51*, 11131–11135.
- (26) Müller, A. J.; Arnal, M. L. *Prog. Polym. Sci.* **2005**, *30*, 559–603.
- (27) Snyder, C. R.; Henry, J. S.; DeLongchamp, D. M. *Macromolecules* **2011**, *44*, 7088–7091.

- (28) Kohn, P.; Huettner, S.; Komber, H.; Senkovskyy, V.; Tkachov, R.; Kiriya, A.; Friend, R. H.; Steiner, U.; Huck, W. T. S.; Sommer, J.-U.; Sommer, M. *J. Am. Chem. Soc.* **2012**, *134*, 4790–4805.
- (29) Ungar, G.; Stejny, J.; Keller, A.; Bidd, I.; Whiting, M. C. *Science* **1985**, *229*, 386–389.
- (30) Koch, F. P. V.; Rivnay, J.; Foster, S.; Müller, C.; Downing, J. M.; Buchaca-Domingo, E.; Westacott, P.; Yu, L.; Yuan, M.; Baklar, M.; Fei, Z.; Luscombe, C.; McLachlan, M. A.; Heeney, M.; Rumbles, G.; Silva, C.; Salleo, A.; Nelson, J.; Smith, P.; Stingelin, N. *Prog. Polym. Sci.* **2013**, *38*, 1978–1989.
- (31) Brinkmann, M.; Rannou, P. *Adv. Funct. Mater.* **2007**, *17*, 101–108.
- (32) Liu, J.; Arif, M.; Zou, J.; Khondaker, S. I.; Zhai, L. *Macromolecules* **2009**, *42*, 9390–9393.
- (33) Crist, B.; Mirabella, F. M. *J. Polym. Sci., Part B: Polym. Phys.* **1999**, *37*, 3131–3140.
- (34) Feller, W. *An Introduction to Probability Theory and Its Applications*, 3rd ed.; Wiley: New York, 1968; Vol. 1.
- (35) Guttman, C. M.; DiMarzio, E. A.; Hoffman, J. D. *Polymer* **1981**, *22*, 1466–1479.
- (36) De Gennes, P.-G. *Scaling Concepts in Polymer Physics*; Cornell University Press: Ithaca, NY, 1979.
- (37) McCulloch, B.; Ho, V.; Hoarfrost, M.; Stanley, C.; Do, C.; Heller, W. T.; Segalman, R. A. *Macromolecules* **2013**, *46*, 1899–1907.
- (38) Singh, C. R.; Gupta, G.; Lohwasser, R.; Engmann, S.; Balko, J.; Thelakkat, M.; Thurn-Albrecht, T.; Hoppe, H. *J. Polym. Sci., Part B: Polym. Phys.* **2013**, *51*, 943–951.
- (39) Mandelkern, L. *Polym. J.* **1985**, *17*, 337–350.